16 DMFT for f-Electron Systems

Bernard Amadon
CEA, DAM, DIF,
Université Paris-Saclay
Laboratoire Matière en Conditions Extrêmes
91680 Bruyères-le-Châtel, France

Contents

1 Introduction to strong correlation: localized (f) orbitals **2**
1.1 Atomic orbitals . . . 2
1.2 Localization/delocalization of electrons . . . 3
1.3 The Hubbard model . . . 4

2 Introduction to DMFT and DFT+DMFT **7**
2.1 Dynamical Mean-Field Theory . . . 7
2.2 DFT+DMFT . . . 12

3 f-electron systems: pure metals **20**
3.1 Lanthanides . . . 20
3.2 Actinides . . . 24

4 f-electron systems: oxides **26**
4.1 Electronic structure of Ce_2O_3 . . . 26
4.2 Magnetic ordering in UO_2 . . . 28

5 Conclusion **28**

E. Pavarini and E. Koch (eds.)
Orbital Physics in Correlated Matter
Modeling and Simulation Vol. 13
Forschungszentrum Jülich, 2023, ISBN 978-3-95806-689-2
http://www.cond-mat.de/events/correl23

In these notes, after a brief introduction to strong correlations and f-orbitals in solid state physics, I will introduce Dynamical Mean-Field Theory (DMFT) and the combination of Density Functional Theory (DFT) and DMFT (See also references [1], [2], and [3]). Then I will discuss some applications of DFT+DMFT on some metals and oxides.

1 Introduction to strong correlation: localized (f) orbitals

1.1 Atomic orbitals

We first focus on the spatial localization of orbitals as a function of their principal quantum numbers: $1s$, $2p$, $3d$ and $4f$ orbitals are orthogonal to lower orbitals only through the angular part because for their value of l, they are the orbitals with the lowest principal quantum number [3]. As a consequence, the radial part of the wavefunction is not constrained by orthogonality, and can lower its Coulomb interaction with the nucleus by being more localized. Thus, these orbitals are more localized than others. Fig. 1 illustrates the localization of $3d$ and $4f$ with respect to $4d$, $5d$ and $5f$ orbitals. Indeed, lanthanides are notorious examples of systems exhibiting very strong correlation effects.
Concerning the angular part, it has more and more nodal planes as l increases, thus in particular, d and f orbitals are fairly localized in space. As a consequence, $4d$, $5d$ and $5f$ orbitals exhibit also important correlation effects.

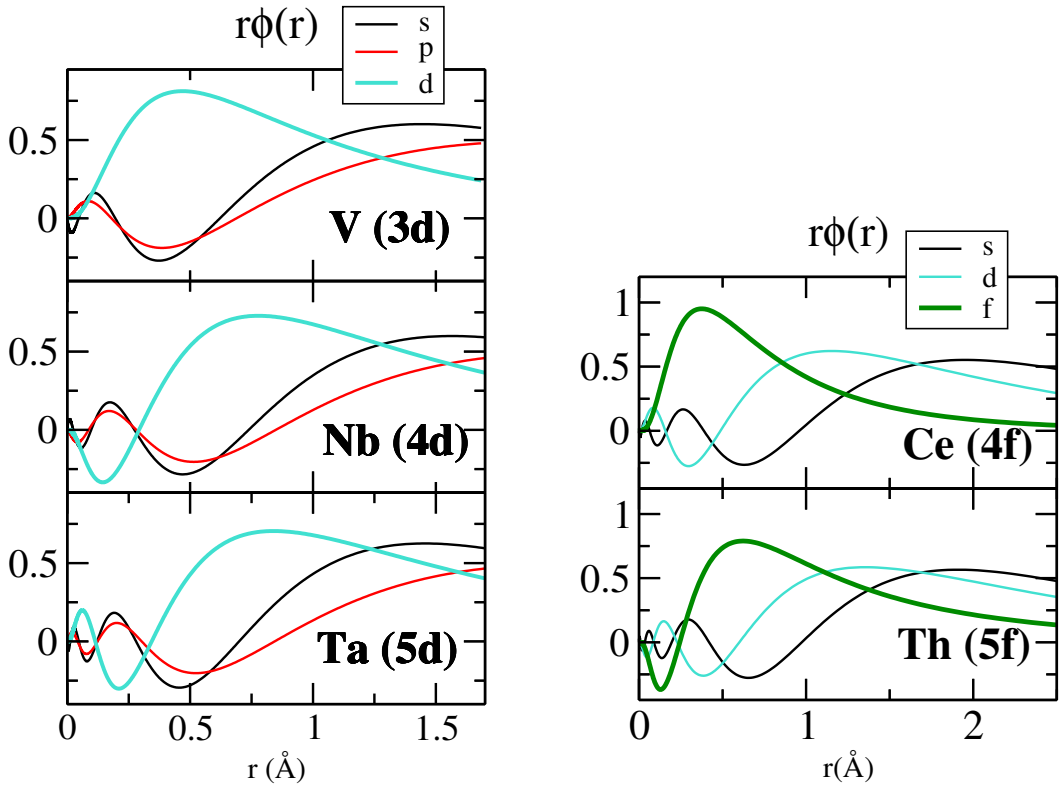

Fig. 1: *Radial part of valence wavefunctions of some atoms (computed in DFT/LDA).*

1.2 Localization/delocalization of electrons

Two main consequences arise from the localization of orbitals:

- When a solid is formed from atoms, the overlap of localized orbitals is weaker than for delocalized orbitals and thus the bandwidth W is smaller (see e.g [4]).
- The more localized the orbitals, the stronger the local interactions "U" between electrons, because electrons are closer to each other.

The simplest example to illustrate these two effects is the formation of the H_2 molecule. In this case, the competition between chemical bonding and interaction leads to a change of the ground state as the interatomic distance increases. At large distances, the electrons are localized each on its atom to avoid the Coulomb interaction with the other electrons (here $U > W$). At small distance, the two electrons delocalize in a bonding molecular orbital.
We see another consequence of this for solids on Fig. 2. It represents the evolution of the volume of pure elements as a function of the number of electrons, for $4d$, $4f$ and $5f$ elements. We now discuss each curve:

- $4d$ orbitals are fairly delocalized, and form bands. Thus, as Z increases, electrons fill the $4d$ band. First the bonding states are filled and then antibonding states. As a consequence, the volume decreases and then increases along the line. This experimental observation is thus coherent with the delocalization of $4d$ electrons.
- For lanthanides, the $4f$ electrons are localized, thus there is a negligible overlap between $4f$ orbitals. As a consequence, adding electrons inside the f-bands has no effect on the cohesion of the crystal. The decrease of the volume is called lanthanide contraction and is due to the poor shielding of nuclear charge by $4f$ orbitals. Eu and Yp have especially large volumes because one bonding electron is transferred to the non-bonding f-shell in order to reach a half-filled or a full f-shell.
- For actinides, the localization appears at the middle of the $5f$ line. One way to understand this is that as Z increases, the $5f$ orbitals are more and more localized because of the attraction with the nucleus. Starting from americium, the system localizes electrons to lower the energy.

This graph suggests that $4f$ electron systems will be closer to the atomic limit. We now discuss the equation of states of the lanthanides as a function of pressure. Refs. [5, 6] show that at ambient pressure and even for moderate pressure, the lanthanides exhibit compact structures. Under pressure, their structure changes becoming more complex and distorted [5, 6]. This suggests that under pressure, f-electrons participate in the bonding as in, e.g., uranium and neptunium (which also have low symmetry equilibrium structures).
We now discuss cerium, which is a model system for lanthanides (see phase diagram in Fig. 3). The α-γ transition in cerium is a first-order isostructural volume collapse transition. The transition line ends at a critical point (CP) around 1.5 GPa and 480 K [7] (see Fig. 3). The (larger

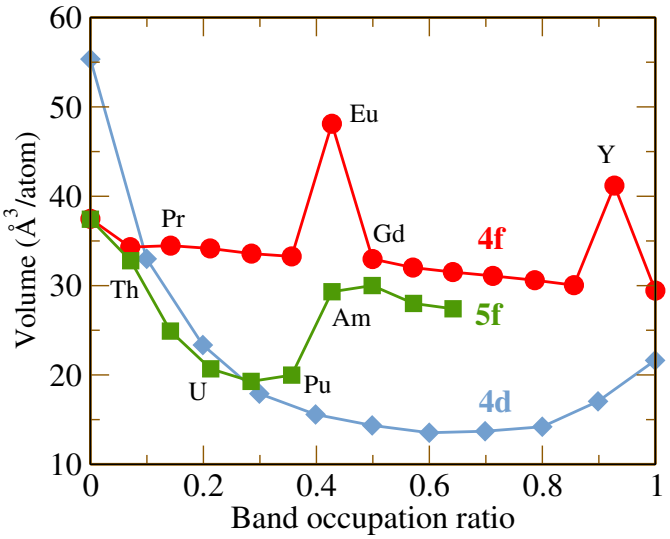

Fig. 2: *Evolution of volume (in Å^3 per atom) of pure elements are a function of the number of electrons for some rows of the periodic table (see also [5]).*

volume) γ-phase exhibits a Curie-Weiss behavior for the magnetic susceptibility while it is Pauli-like in the (smaller volume) α-phase (see Fig. 17). This is interpreted as $4f$ electrons, being localized in the γ-phase, giving rise to local moments and contributing weakly to the electronic bonding, whereas in the α-phase, the $4f$ electrons participate in both bonding [8] and formation of quasi-particles as shown in photoemission spectra [9, 10]. The $\alpha \rightleftharpoons \gamma$-phase transition of Ce is hence a model system for a volume collapse phase transitions due to the delocalization of localized electrons under an increase of pressure or decrease of temperature (see Fig. 3 for other examples in the lanthanides). This is a difference between cerium and other systems, such as praseodymium and plutonium [4], in which the volume collapse occurs directly from the compact structure to lower symmetry structures.

1.3 The Hubbard model

In this section, we will study the Hubbard model, which is appropriate to model the localization/delocalization competition. Using second quantization, one can write the Hamiltonian as

$$H = \sum_i \langle i|h|j\rangle \, c_i^\dagger c_j + \sum_{i,j,k,l} \langle ij|v|kl\rangle \, c_i^\dagger c_j^\dagger c_k c_l \tag{1}$$

In this equation, i, j, k, l belong to a complete one particle basis. If the sums in this equation are restricted to only one orbital per atoms, and if only on site interactions are kept, one recovers the Hubbard model

$$H = \sum_{i \neq j} t_{ij} c_i^\dagger c_j + \sum_i \varepsilon_0 (n_{i\uparrow} + n_{i\uparrow}) + \sum_i U n_{i\uparrow} n_{i\downarrow} \tag{2}$$

In this equation, as we have only one orbital per site, i, j refers to atomic sites. We will now try to understand two limits of this Hamiltonian.

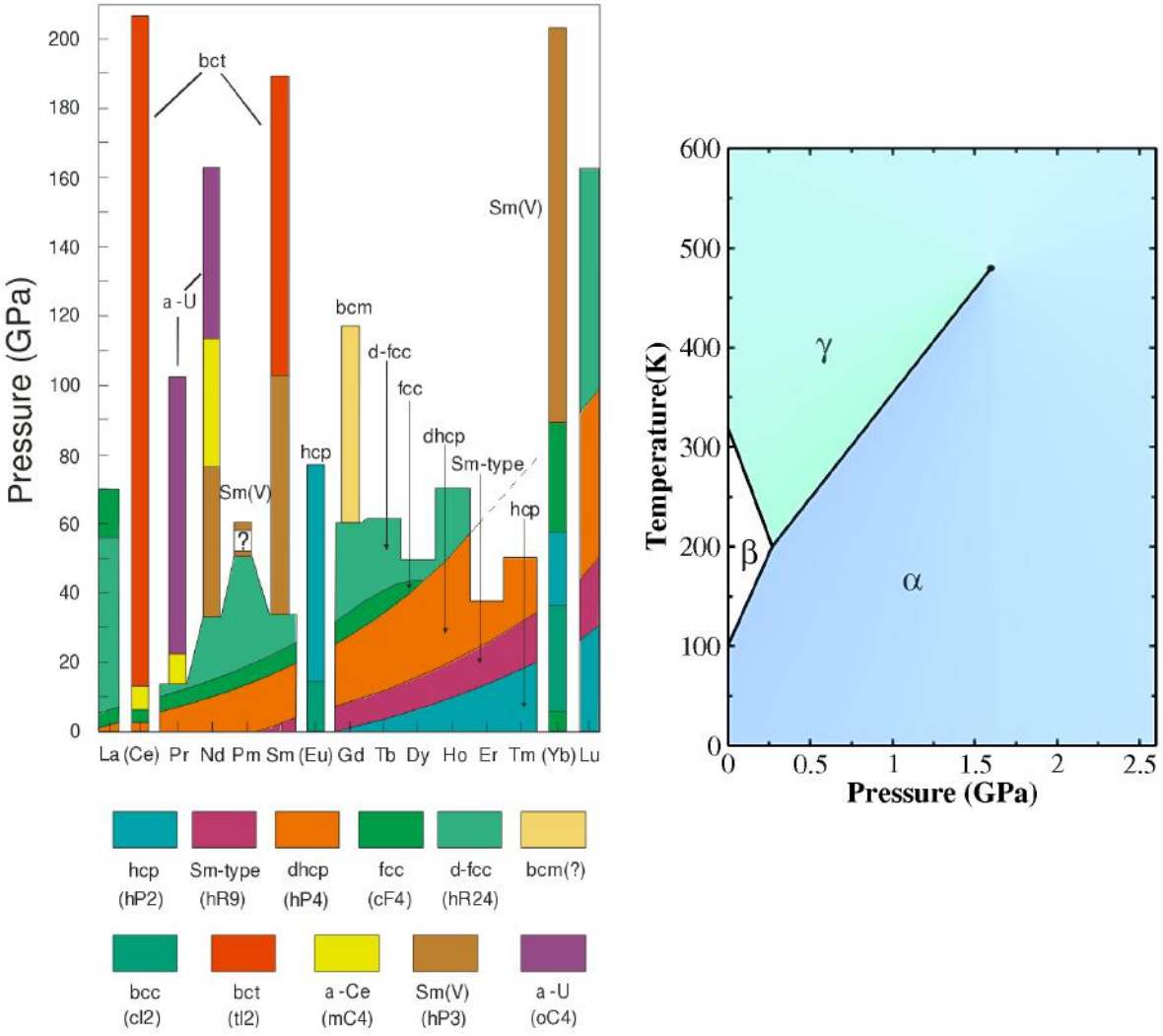

Fig. 3: *Left: Phases of the lanthanides as a function of pressure (From [6]). Right: Phase diagram of cerium.*

1.3.1 Delocalization limit: $U/t \ll 1$

In this limit, we neglect the interaction term.

$$H = \sum_{j \neq i} t_{ij} c_i^\dagger c_j + \varepsilon_0 (n_{i\uparrow} + n_{i\downarrow}) \tag{3}$$

One can easily solve this non-interacting Hamiltonian either by direct diagonalization or by using Bloch states: We can define Bloch states $|k\rangle$ as

$$|k\rangle = \frac{1}{\sqrt{N}} \sum_i |T_i\rangle \, \mathrm{e}^{ikT_i} \tag{4}$$

where $|T_i\rangle$ are atomic orbitals: $\langle r|T_i\rangle = \varphi(r - T_i)$ on site i. We also have

$$|T_i\rangle = \frac{1}{\sqrt{N}} \sum_k |k\rangle \mathrm{e}^{-ikT_i} \tag{5}$$

and the change of basis for creation and annihilation operators

$$c_i^\dagger = \frac{1}{\sqrt{N}} \sum_k c_k^\dagger \mathrm{e}^{-ikT_i} \qquad c_i = \frac{1}{\sqrt{N}} \sum_k c_k \mathrm{e}^{ikT_i}. \tag{6}$$

As a consequence, one can show that

$$H = \sum_k \varepsilon_k c_k^\dagger c_k \quad \text{with} \quad \varepsilon_k = \frac{1}{N} \sum_{ij} t_{ij} \mathrm{e}^{-ik(T_i - T_j)}. \tag{7}$$

In a simple case (one dimension and if t_{ij} is non-zero only for neighboring atoms), we have (note that t is negative) the following dispersion relation which gives the energy of levels as a function of the value of k.

$$\varepsilon_k = \varepsilon_0 + 2t\cos(ka) \tag{8}$$

According to the Bloch theorem, k must belong to the first Brillouin Zone $[-\frac{\pi}{a}, \frac{\pi}{a}]$, where a is the distance between the atoms. We now suppose that we have one electron per atom, whereas there are two states per atoms. As a consequence, the band is half filled. The system is thus metallic and the Fermi levels is at ε_0.

1.3.2 Localization limit: $U/t \gg 1$

$$H = \sum_i U n_{i\uparrow} n_{i\uparrow} + \sum_i \varepsilon_0 (n_{i\uparrow} + n_{i\downarrow}) \tag{9}$$

In this case, the Hamiltonian is a sum of Hamiltonians for independent atoms! We thus have to solve the atomic problem. The size of the Hilbert space for this system is four (2^2) and the states for each number of electrons per atom are

- 0 electron: $|0\rangle : E = 0$
- 1 electron: $|\uparrow\rangle$ and $|\downarrow\rangle$: $E = \varepsilon_0$
- 2 electrons: $|\uparrow\downarrow\rangle$: $E = 2\varepsilon_0 + U$

Let us now suppose that the system has one electron per atom. From the above energies, one can compute the cost associated to the hopping of one electron from one atom to another atom (see Fig. 4). The cost is U. The order of magnitude of U in a real system is a few eV. As a consequence, at room temperature, electrons will be localized and the system is called a Mott insulator. The insulating character comes from interactions and not from a band structure effect. One can also compute the photoemission spectra, i.e., the energy to add ($E(|\uparrow\downarrow\rangle) - E(|\uparrow\rangle) = \varepsilon_0 + U$) or remove ($E(|\uparrow\rangle) - E(|0\rangle) = \varepsilon_0$) an electron. We see that the photoemission spectra (or spectral function) will have two peaks located at ε_0 and $\varepsilon_0 + U$. The two peaks are separated by U, which is thus the photoemission gap. These peaks correspond to the Hubbard bands.

1.3.3 The Mott transition

From these two limits, one can deduce that as U/t will increase, the systems will change from a metal to a Mott insulator. This is the phenomenon of the Mott transition. But we need an approximation to find the solution for intermediate U/t. This is one of the purposes of DMFT.

Fig. 4: *For $U/t \gg 1$, the cost of a hopping is $E(|\uparrow\downarrow\rangle) + E(|0\rangle) - 2E(|\uparrow\rangle) = U$*

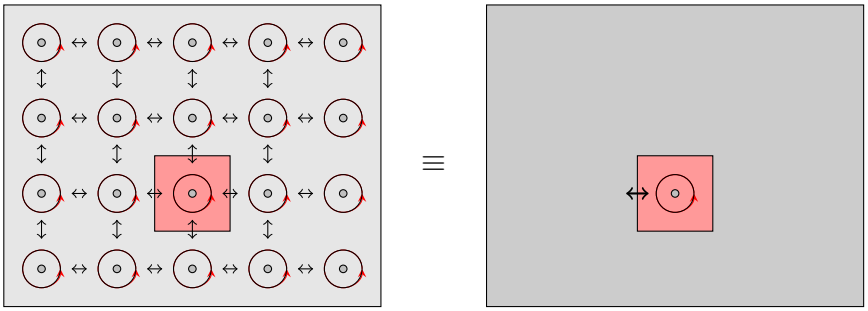

Fig. 5: *In DMFT, the Hubbard model is simplified by an Anderson model. On the left, the Hubbard model is represented schematically. On the right, one atom in red is interacting with the effective field of the others.*

2 Introduction to DMFT and DFT+DMFT

2.1 Dynamical Mean-Field Theory

2.1.1 The Anderson model

We would like to describe correctly the on-site Coulomb interactions which are essential to describe the atomic limit. The first idea of DMFT is to mimic the Hubbard model by a correlated atom with the exact Coulomb interaction, embedded in a bath of uncorrelated orbitals (see Fig. 5). The effect of all the other atoms are gathered in the bath. This is an Anderson model [11] whose Hamiltonian writes

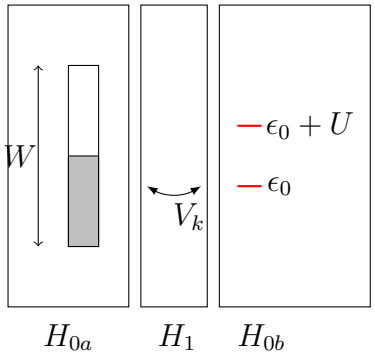

$$H_{\text{Anderson}} = \underbrace{\sum \omega_k \, a^\dagger_{k,\sigma} a_{k\sigma}}_{H_{0a}} + \underbrace{\sum_{k,\sigma} V_k \left(a^\dagger_{k,\sigma} c_\sigma + c^\dagger_\sigma a_{k,\sigma} \right)}_{H_1} + \underbrace{\varepsilon_0 (n_\uparrow + n_\downarrow) + U n_\uparrow n_\downarrow}_{H_{0b}} \tag{10}$$

The use of the Anderson model is a mean-field idea that goes beyond static mean field. Indeed, we do not have only one electron in an effective field as in usual static mean-field theory, but a whole many-body atom whose interactions are taken into account exactly. Moreover the Anderson model will be defined self-consistently, but we will discuss this in the next section. In this section we just focus on the physics of the Anderson model. Once again, we are going to investigate several limiting cases for this Hamiltonian

The isolated atom limit: $V_k = 0$. This case is identical to the limit $U/t \gg 1$ of the Hubbard model: the correlated atom is insulating.

The $U = 0$ limit. The hamiltonian writes

$$H_{\text{Anderson}} = \sum \omega_k \, a^\dagger_{k,\sigma} a_{k\sigma} + \sum_{k,\sigma} V_k \left(a^\dagger_{k,\sigma} c_\sigma + c^\dagger_\sigma a_{k,\sigma} \right) + \varepsilon_0 (n_\uparrow + n_\downarrow).$$

This is again a non-interacting system which can be solved easily: The atomic level will hybridize with the levels at ω_k, and will acquire a width.
Let us compute the Green function of this system. We can use the equation of motion of the (non-interacting) Green function, we thus have

$$\big(\omega I - H\big) G = I. \tag{11}$$

The dimension of these matrices is equal to $N+1$. It contains the N uncorrelated orbitals ω_k and the correlated orbital ε_0. The diagonal elements of H are the energies ω_k and ε_0. The only off diagonal terms are the coupling elements of the level at ε_0 to the levels at ω_k.

$$H = \begin{pmatrix} \varepsilon_0 & V_1 & \cdots & V_k & \cdots & V_N \\ V_1 & \omega_1 & 0 & 0 & 0 & 0 \\ \vdots & 0 & \ddots & 0 & 0 & 0 \\ V_k & 0 & 0 & \omega_k & 0 & 0 \\ \vdots & 0 & 0 & 0 & \ddots & 0 \\ V_N & 0 & 0 & 0 & 0 & \omega_N \end{pmatrix}$$

We can easily invert this matrix and compute the Green function of the correlated orbital (Using $A^{-1} = \mathrm{Com}(A)^T / \mathrm{det} A$ to invert $\omega I - H$). We obtain

$$G(\omega) = \frac{1}{\omega - \varepsilon_0 - \Delta(\omega)} \qquad \text{with} \quad \Delta(\omega) = \sum_k \frac{V_k^2}{\omega - \omega_k} \tag{12}$$

Where $\Delta(\omega)$ is called the hybridization function.
We can now compute the spectral function of this system by computing:

$$A(\omega) = -\frac{1}{\pi} \mathrm{Im} G^R(\omega + i\delta) \tag{13}$$

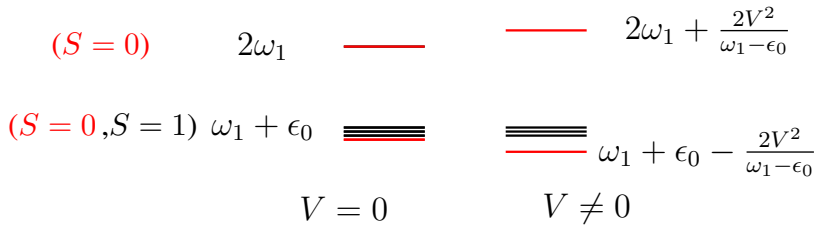

Fig. 6: *Two electrons levels with $V=0$ and V small.*

We need[1]

$$\Delta(\omega+i\delta) = \sum_k \frac{V_k^2}{\omega-\omega_k} - i\pi \sum_k |V_k|^2\, \delta(\omega-\omega_k) \tag{14}$$

If $\Delta = 0$, then the spectral function has a peak at ε_0. Using the last two equations, the peak at ε_0 in the spectral function will be shifted by the real part of Δ and will be broadened by the imaginary part of Δ. Interestingly, the imaginary part of Δ recovers the Fermi golden rule (width of the level coupled to the continuum is $\pi \sum_k |V_k|^2\, \delta(\omega-\omega_k)$).

The Anderson Molecule. We now simplify the bath by replacing it by a single level. We reproduce here the example detailed in Ref. [12, 13].
We suppose that U is infinite, so a double occupation of the localized level is impossible. Finally we limit our study to the states with 2 electrons. With these constraints, we have 5 possible states in the Hilbert space: the first is the double occupation of the bath level (this is a state with S=0) and there are four states with one electron in the bath level and one electron in the localized level. Among these four states, there are one triplet (S=1) and one singlet (S=0). If $V=0$, then the four levels are degenerate. In Fig. 6, the singlet states are in red.
If the hybridization V is non-zero, then the two states with S=0 couple (see Fig. 6). As a consequence we have a possible transition between the singlet and the triplet state at very low energy. This phenomenon has the same physical origin as the Kondo effect. It shows that a resonance exists even in a very strongly correlated system (U large) and this resonance will be at the Fermi level. We can define a temperature T^* corresponding to the difference of energy between the singlet and triplet state. Below this temperature, the system will exhibit the resonance, which will fade as temperature increases. Moreover, below this temperature, the magnetic moment of the localized level is completely cancelled by the formation of the singlet state.

2.1.2 The self consistency condition and the DMFT loop

Following the definition of the Green function in the local orbital basis (i and j)

$$G_{ij}(t) = -i\langle N|T(c_i^\dagger(t)c_j(0)|N\rangle \tag{15}$$

[1] We use $\lim_{\delta\to 0} \frac{1}{\pi}\frac{\delta}{x^2+\delta^2} = \delta(x)$.

one can compute the Bloch Green function

$$G_{\mathbf{k}}(t) = \frac{1}{N} \sum_{ij} \mathrm{e}^{i\mathbf{k}(T_i - T_j)}\, G_{ij}(t) \tag{16}$$

thus, in frequency

$$G_{\mathbf{k}}(\omega) = \frac{1}{N} \sum_{ij} \mathrm{e}^{i\mathbf{k}(T_i - T_j)}\, G_{ij}(\omega) \tag{17}$$

Using the equation of Motion of the Green function $(\omega - H - \Sigma)G = 1$, the lattice Green function for the Hubbard model is written

$$G_{\mathbf{k}}(\omega) = \frac{1}{\omega - \varepsilon_{\mathbf{k}} - \Sigma_{\mathbf{k}}(\omega)}\,, \tag{18}$$

where the self-energy is unknown. The local Green function of the lattice is

$$G_{ii}(\omega) = \frac{1}{N} \sum_{\mathbf{k}} \mathrm{e}^{ik(T_i - T_i)}\, G_{\mathbf{k}}(\omega) = \frac{1}{N} \sum_{\mathbf{k}} G_{\mathbf{k}}(\omega). \tag{19}$$

Besides, the Green function for the Anderson impurity model is

$$G_{\text{Anderson}}(\omega) = \frac{1}{\omega - \varepsilon_0 - \Delta(\omega) - \Sigma(\omega)}\,. \tag{20}$$

The DMFT idea [1] is to identify the local Green function of the Hubbard model with the Green function of Anderson model and the self-energy of the Hubbard model to be equal to the self-energy of the Anderson model:[2] it is the *self-consistency relation* of DMFT. This implies in particular that the local one particle excitations of the Hubbard model will be the same as the one particle excitations of the Anderson model. This writes

$$\frac{1}{N} \sum_{k} \frac{1}{\omega - \varepsilon_{\mathbf{k}} - \Sigma(\omega)} = \frac{1}{\omega - \varepsilon_0 - \Delta(\omega) - \Sigma(\omega)}\,. \tag{25}$$

[2] Thus we have expressed also the self-energy in the Bloch basis. We start from the expression of the self-energy as a sum of local self-energies on different sites

$$\Sigma = \sum_{T_i} |T_i\rangle \Sigma(\omega) \langle T_i| \tag{21}$$

We use then

$$|T_i\rangle = \frac{1}{\sqrt{N}} \sum_{\mathbf{k}} |\mathbf{k}\rangle \mathrm{e}^{-i\mathbf{k}T_i} \tag{22}$$

Thus by replacing the last equation in Eq. (21), we have

$$\Sigma = \sum_{\mathbf{k}} |\mathbf{k}\rangle \Sigma(\omega) \langle \mathbf{k}'| \tag{23}$$

Thus

$$\langle \mathbf{k}|\Sigma|\mathbf{k}\rangle = \Sigma(\omega) \tag{24}$$

Thus for a local self-energy, the self-energy in the basis of Bloch states is equal to the local self-energy.

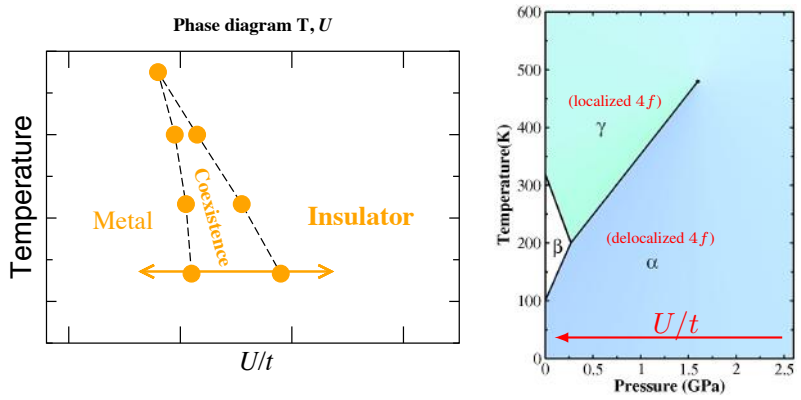

Fig. 7: *Phase diagram of the Hubbard model in DMFT compared to that of Cerium.*

This equation enables us to find $\Delta(\omega)$ as a function of the self-energy: $\Delta = \Delta[\Sigma]$ and also $\varepsilon_0 = \frac{1}{N}\sum_{\mathbf{k}} \varepsilon_{\mathbf{k}}$.[3] Besides, the solution of the Anderson model enables us to have the self energy from the value of ε_0 and Δ.[4] So this creates a system of two equations that can be solved self-consistently. These two equations constitute the DMFT self-consistent loop that can be solved by iteration.

2.1.3 The Hubbard model in DMFT

The main results for the Hubbard model phase diagram in DMFT (in infinite dimension, without magnetism and for one electron per atom) are summed up on Figs. 7 and 8. First, the metal insulator transition is a first-order phase transition. Moreover, the paramagnetic insulating phase with a degeneracy of two can be described in contrary to the static mean-field approximation which breaks the symmetry and creates magnetism.

We now describe the evolution of the spectral function. At large value of U, the Hubbard bands are present but still broadened by hybridization. Then, a resonance peak appears at the Fermi level and grows, as U/t decreases. Importantly thus, the metallic phase appears whereas the Hubbard band are still present in the photoemission spectra. Such feature is also not described by the static mean-field approximation. Let us finally outline that in DMFT, both the atomic limit ($U/t \gg 1$) and the delocalization limit ($U/t \ll 1$) are exact.

We compare on Figs. 7 and 8 the physics of the Hubbard model to the physics of an f electron system, namely pure cerium. As was discussed above, pure cerium exhibits two phases, one with delocalized f-electrons and one with localized electrons and the transition between these two phases can be controlled with pressure or temperature. It can be rationalized in comparison to Hubbard model: applying pressure is equivalent to reducing t. Besides, phases of cerium both exhibit Hubbard bands. The α-phase, exhibits less intense Hubbard band and larger quasi-particle peak, as expected for more delocalized electrons. In the next section, we will discuss DFT+DMFT in order to apply DMFT ideas to a real system such as cerium.

[3] Equivalently, one can say that the non-interacting Green function $\mathcal{G}_0^{-1} = \omega - \varepsilon_0 - \Delta(\omega)$ can be obtained from the self-energy.

[4] Equivalently, one can obtain the Green function and the self energy of the Anderson model as a function of the non-interacting Green function

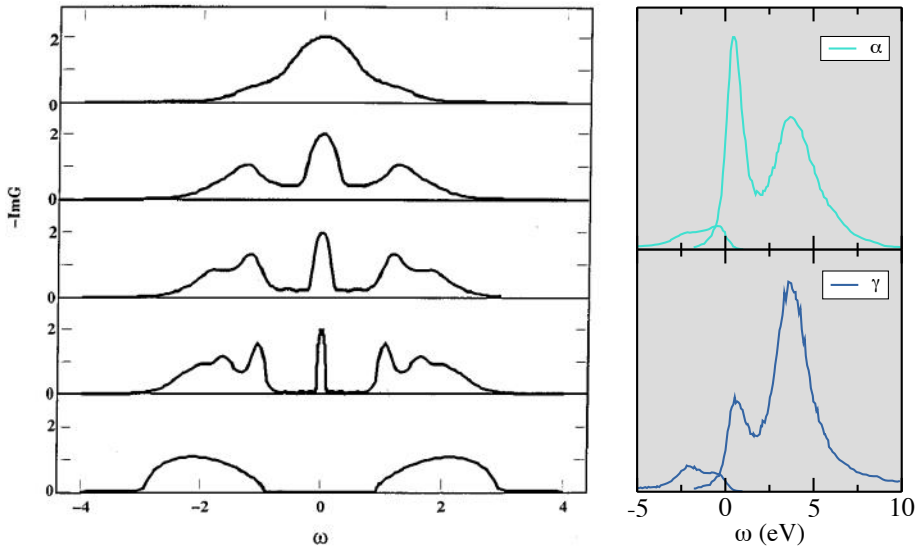

Fig. 8: *Evolution of the spectral function in the Hubbard model (from Ref [1]) compared to photoemission spectra in cerium (From Ref. [9, 10])*

2.2 DFT+DMFT

The rough idea of DFT+DMFT is to use the DFT/LDA Hamiltonian to define the one body term of the Hubbard model and then supplement it by an exact Coulomb interaction for the correlated orbital subset. However, to apply DMFT ideas to a real system, one need first to define correlated orbitals [14–16] and a corresponding value of the effective interaction U [17]. This is important and is discussed in the next subsection. I just outline here that there is no unique way to define correlated orbitals. So several choices have been made in the literature. They include atomic orbitals, or Wannier orbitals. When the choice of correlated orbitals is done, the effective interaction for these orbitals has to be computed. One formalism is the constrained Random Phase Approximation (cRPA) method [17] which considers that the effective interaction between correlated electrons is the bare interaction screened by all the non-correlated electrons. It thus requires the calculation of a non-interacting polarizability and the inverse dielectric function. It is described in the second subsection.

Then, using correlated orbitals and related values of U, a DFT+DMFT calculation can be carried out. The scheme will be presented in the third subsection. Lastly, I will briefly discuss solvers for the Anderson model in the fourth subsection.

2.2.1 Correlated orbitals: how to define them?

In this section, we briefly discuss Wannier functions, which are a flexible tool to define correlated orbitals.

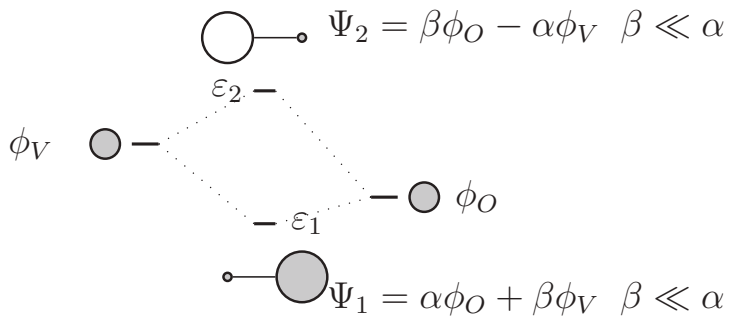

Fig. 9: *Simple molecular orbital diagram for an diatomic molecule containing an electropositive atom (V) and an electronegative atom (O). It can be viewed as a simple model for $SrVO_3$ or UO_2 or Ce_2O_3. In the text, we use this model with 3 electrons: the ε_2 level is thus half-filled.*

Projected Local Orbitals Wannier functions and Maximally Localized Wannier functions. Projected Wannier functions are defined in Refs. [14, 16]. We first introduce the auxiliary wavefunctions $|\tilde{\chi}^{\mathbf{R}}_{\mathbf{k}m}\rangle$ as

$$|\tilde{\chi}^{\mathbf{R}}_{\mathbf{k}m}\rangle \equiv \sum_{\nu\in\mathcal{W}} |\Psi^{\sigma}_{\mathbf{k}\nu}\rangle\langle\Psi^{\sigma}_{\mathbf{k}\nu}|\chi^{\mathbf{R}}_{\mathbf{k}m}\rangle. \tag{26}$$

For a given atomic site $\mathbf{R}$, we call $|\chi^{\mathbf{R}}_{\mathbf{k}m}\rangle$ the Bloch transform of isolated atomic orbitals with projected angular momentum m. $|\Psi^{\sigma}_{\mathbf{k}\nu}\rangle$ are the Kohn-Sham orbitals for k-point $\mathbf{k}$, band index ν and spin σ. $|\tilde{\chi}^{\mathbf{R}}_{\mathbf{k}m}\rangle$ is thus a weighted sum of Kohn-Sham orbitals. This sum extends over a given number of Kohn-Sham orbitals that can be defined by an index range or alternatively by an energy window $\mathcal{W}$. For a finite $\mathcal{W}$, the orthonormalization of $|\tilde{\chi}^{\mathbf{R}}_{\mathbf{k}m}\rangle$ leads to well defined Wannier functions $|w^{\mathbf{R}}_{\mathbf{k}m}\rangle$, unitarily related to $|\Psi^{\sigma}_{\mathbf{k}\nu}\rangle$ by[5]

$$|w^{\mathbf{R}}_{\mathbf{k}m}\rangle = \sum_{\nu\in\mathcal{W}} |\Psi^{\sigma}_{\mathbf{k}\nu}\rangle\langle\Psi^{\sigma}_{\mathbf{k}\nu}|w^{\mathbf{R}}_{\mathbf{k}m}\rangle. \tag{27}$$

It is important to notice that the localization of $|w^{\mathbf{R}}_{\mathbf{k}m}\rangle$ will decrease if $\mathcal{W}$ decreases. Maximally localized Wannier functions are Wannier functions whose extension is minimized [18]. They have the advantage over projected local orbital Wannier functions that they are uniquely defined.

Wannier functions: a pedagogical simplified molecular model In order to illustrate the localization of Wannier functions, we consider a simple diatomic molecule containing an electropositive atom (V) and an electronegative atom (O). In this model molecule, we consider only one orbital per atom, and for simplification, we assume it is of s symmetry. It can be viewed as a very simple model for $SrVO_3$ or UO_2. The bonding state at ε_1 is the analogue of the O-p like band, whereas the antibonding state at ε_2 is the analogue of the V-d like bands.

We now suppose that the system contains 3 electrons. The V-like band is thus half filled. We use Eq. (26) with $\chi = \phi_V$ to compute Wannier functions for two energy windows:

[5] In the limit of a infinite number of Kohn-Sham bands, the projection in Eq. (26) becomes complete and the Wannier functions $|w^{\mathbf{R}}_{\mathbf{k}m}\rangle$ become equivalent to atomic orbitals $|\chi^{\mathbf{R}}_{\mathbf{k}m}\rangle$.

Eigenstates included in the energy window $\mathcal{W}$	$\{\varepsilon_2\}$	$\{\varepsilon_1, \varepsilon_2\}$
Corresponding Wannier function w_V	$\|\Psi_2\rangle$	$\|\phi_V\rangle$
Corresponding number of electrons n_V	1	$2\beta^2+\alpha^2$

Table 1: *Wannier function on vanadium and corresponding numbers of electron in a simple diatomic molecule for two different choices of the energy window.*

- If $\mathcal{W} = \{\varepsilon_2\}$, then Eq. (26) contains only one term: $|\widetilde{\chi}\rangle = |\Psi_2\rangle\langle\Psi_2|\phi_V\rangle = \alpha|\Psi_2\rangle$. After renormalizing $\widetilde{\chi}$, we find that the Wannier function is a molecular orbital $|w_V\rangle = |\Psi_2\rangle$ that contains an oxygen contribution. The number of electrons in this orbital is 1.

- If $\mathcal{W} = \{\varepsilon_1, \varepsilon_2\}$, then Eq. (26) contains two terms. One shows easily that the Wannier function is a localized atomic orbital $|w_V\rangle = |\phi_V\rangle$ and is thus much more localized than in the previous case. The number of electrons in $2\beta^2+\alpha^2 \neq 1$.

So this simple example illustrates how the localization of the Wannier functions is modified by the choice of the energy windows of Kohn-Sham bands. A similar illustration in the case of $SrVO_3$ can be seen in [15]. We will now discuss the calculation of effective interactions for these orbitals.

2.2.2 How to compute the effective coulomb interaction?

There are several ways to compute effective interactions [19, 20, 17]. Here, we will briefly present the constrained random phase approximation method [17, 21] (cRPA) which is particularly adapted to DFT+DMFT.
The cRPA method depends on the definition of a many-body model [21]. The many-body model is defined by a set of local orbitals together with the interactions among them. A cRPA calculation of a model would require first the definition of a set of local orbitals, and second a consistently calculated screened interaction: it considers that the effective interaction between correlated electrons is the bare interaction screened by all the non-correlated electrons. Importantly, thus the value of effective interactions depends on the definition of correlated orbitals discussed above.

The cRPA method We call here χ_0 the non-interacting (Kohn-Sham) polarizability of the system. Let's now separate the correlated states (They could be f-states but the method is more general and correlated orbitals could gather several orbitals from, e.g., different atoms) from the rest (r). We thus have [17]

$$\chi_0 = \chi_0^{\text{correl}} + \chi_0^r. \tag{28}$$

Thus, we can rewrite the inverse dielectric matrix as

$$\epsilon^{-1} = \frac{1}{1 - v(\chi_0^{\text{correl}}+\chi_0^r)}\,. \tag{29}$$

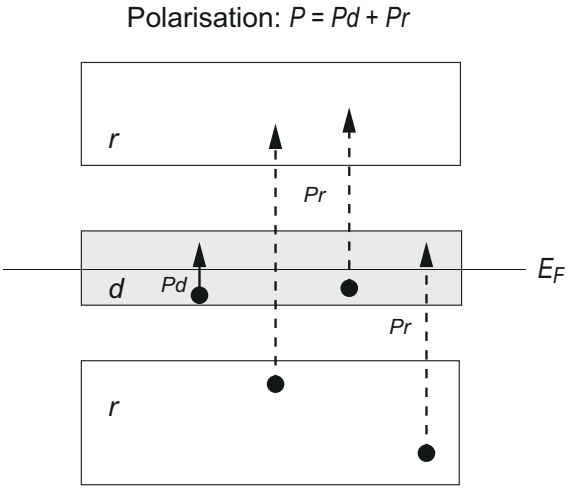

Fig. 10: *Schematic density of states with the transitions that are involved in the polarizability of correlated electrons $P_d \hat{=} \chi_0^{correl}$ and the other transitions that are involved in $P_r \hat{=} \chi_0^r = P - \chi_0^{correl}$ (From [22]).*

We now define the dielectric functions due to non-correlated electrons and the corresponding screened interaction

$$\epsilon_r^{-1} \hat{=} \frac{1}{1 - v\chi_0^r} \quad \text{and} \quad W_r = \epsilon_r^{-1} v = \frac{v}{1 - v\chi_0^r} \,. \tag{30}$$

The dielectric function due to correlated electrons acting on W_r is thus

$$\epsilon_{\text{correl}}^{-1} \hat{=} \frac{1}{1 - W_r \chi_0^{\text{correl}}} \,. \tag{31}$$

With these definitions, one shows that

$$\epsilon_{\text{correl}}^{-1} \epsilon_r^{-1} = ... = \frac{1}{1 - v\chi_0^r - v\chi_0^{\text{correl}}} = \epsilon^{-1} \quad \text{and thus} \quad W \hat{=} \epsilon^{-1} v = \epsilon_{\text{correl}}^{-1} \epsilon_r^{-1} v. \tag{32}$$

The fully screened RPA interaction is the combination of two screening processes. First, the bare interaction is screened by non-correlated electrons (r), giving rise to a screened interaction W_r. Secondly, the screening of this interaction by correlated electrons recovers the fully screened interaction [17].

The main idea of cRPA is to use this separation of screening processes. The screened interaction W_r can be computed explicitly, using the equation written above, which is valid for electrons interacting only with the Hartree potential. Removing the screening by correlated electrons is easy in cases where the correlated orbitals are unitarily related to an isolated set of bands (see Fig. 10). In other cases, several schemes have been proposed.

Then the interaction in the basis of correlated orbitals is computed with

$$U_{1234}(w) = \langle w_1 w_2 | W_r(w) | w_3 w_4 \rangle. \tag{33}$$

Finally, the screening by correlated electrons is explicitly taken into account by solving exactly the correlations with the interaction U_{1234} by a dedicated method (e.g. DMFT).

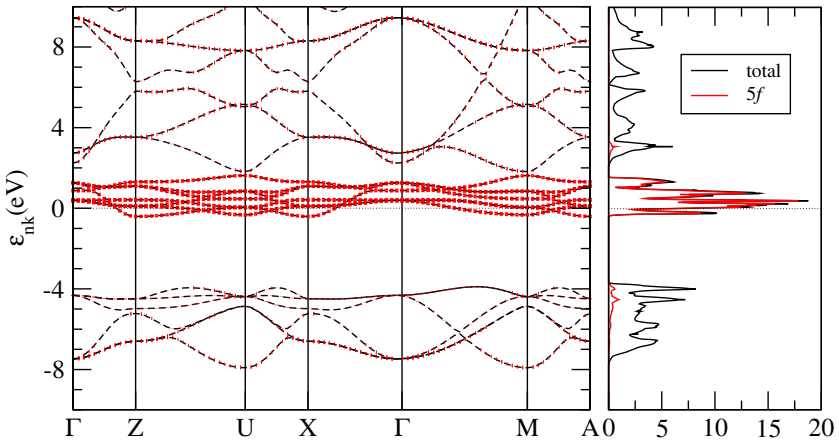

Fig. 11: *Band structure of UO_2 in DFT/LDA [23]. Between –8 eV and –3 eV, bands are mainly O-p like. Then, there are 14 bands of $5f$ character that are at the Fermi level. If Wannier correlated orbitals are constructed only with f-like bands, then, the cRPA interactions can be computed by removing transitions inside the 14 isolated f-bands.*

Many-body models We now briefly consider different kinds of models as discussed in Ref. [21, 25] in the case of UO_2. UO_2 is a paramagnetic insulator above the Néel temperature of 30 K with the fluorine structure.

- f-f model: The model is built from the U-f like bands only: Wannier functions are built from U-f like bands and transitions among the U-f like bands define χ^{correl}.
- fp-fp model: The model is built from the U-f like and O-p like bands. Wannier functions are build from U-f like bands and O-p like bands and transitions among these bands define χ^{correl}. In this case, effective interactions U_{ff}, U_{fp} and U_{pp} can be computed and used in a calculation using explicitly all these interactions.

We now first discuss the value of the interactions. We can first compare the bare interactions for $SrVO_3$ (19.1 eV), cerium (24 eV) and UO_2 (16.1 eV) [23]. It highlights the large localization of orbitals in lanthanides and the fact that interactions in actinides are lower.
We now discuss effective interactions U. The value of U depends largely on the model [23]. It is larger in the fp mode. This comes from the fact that the orbitals are more localized in the fp model and also that screening is lower. Ref [24] discusses the appropriate choice of U in uranium. However, it is expected to be between 4 and 6 eV in UO_2 to reproduce spectral properties [26]. In lanthanides, the values of U required to describe experiments are larger.

model	v	U
f-f	16.0	3.4
fp-fp	17.1	6.2

Table 2: *Bare (v), and cRPA (U) Coulomb interactions for UO_2 computed for different models. Results are from [23] (see also [24])*

2.2.3 The DFT+DMFT scheme

We now suppose that correlated orbitals and effective interactions are defined. We now discuss the DFT+DMFT scheme. In a first step, we are going to write the expression of the lattice Green function for the solid with a local self-energy. The self-energy will later be the DMFT self-energy.

The lattice Green function In comparison to the case of the one-band Hubbard model,

- the number of correlated orbitals is larger (14 for f-elements),
- the number of bands in the system is large, and larger than the number of correlated orbitals because some orbitals are not correlated. For example, in cerium, the $4f$ orbitals are correlated but the $6s$ are not. However, $6s$ and $4f$ states are strongly mixed in the DFT/LDA density of states.

We are going to express all quantities (G, Σ) in the Kohn-Sham wavefunctions basis because the DFT Hamiltonian has a simple expression in this basis

$$H_{\text{LDA}} = \sum_{n\mathbf{k}} |\Psi_{\mathbf{k}n}\rangle \, \varepsilon_{n\mathbf{k}} \, \langle \Psi_{\mathbf{k}n}| \,. \tag{34}$$

The self-energy in DMFT is local and is computed in the local basis (of correlated orbitals), thus the self energy operator is a sum of identical self-energies on each correlated site (m and m' are the quantum numbers of the projection of the angular momentum)

$$\Sigma = \sum_{mm'\mathbf{T}_i} |\chi_{\mathbf{T}_i m}\rangle \, \Sigma_{m,m'}(\omega) \, \langle \chi_{\mathbf{T}_i m'}| \,. \tag{35}$$

We can define the Bloch transform of the localized functions $\chi_{\mathbf{T}_i m}$ as before as

$$|\chi_{\mathbf{T}_i m}\rangle = \frac{1}{\sqrt{N}} \sum_{\mathbf{k}} |\chi_{\mathbf{k}m}\rangle \, \mathrm{e}^{-i\mathbf{k}\mathbf{T}_i}. \tag{36}$$

Thus by replacing the last equation in Eq. (35), we have

$$\Sigma = \sum_{mm'\mathbf{k}} |\chi_{\mathbf{k}m}\rangle \, \Sigma_{m,m'}(\omega) \, \langle \chi_{\mathbf{k}m'}| \,. \tag{37}$$

It can be expressed in the Kohn-Sham basis directly using the fact that $\langle \Psi_{\mathbf{k}n} | \chi_{\mathbf{k}'m} \rangle$ is zero if $\mathbf{k}$ and $\mathbf{k}'$ are different,

$$\Sigma_{nn'}(\mathbf{k}, \omega) = \sum_{m,m'} \langle \Psi_{\mathbf{k}n} | \chi_{\mathbf{k}m} \rangle \, \Sigma_{mm'}(\omega) \, \langle \chi_{\mathbf{k}m'} | \Psi_{\mathbf{k}n'} \rangle. \tag{38}$$

In order to avoid a double-counting of the correlation for correlated orbitals, the self-energy has to contain a so called "double-counting term" which should cancel the DFT/LDA Hartree and exchange-correlation potential for the correlated electrons

$$\Sigma = \Sigma_{\text{DMFT}} - \Sigma_{\text{DC}}. \tag{39}$$

The Green function will obey the usual equation of motion:

$$\big(\omega I - H - \Sigma\big) G = I. \tag{40}$$

Thus the Green function is

$$G_{nn'}(\mathbf{k},\omega) = \big(\omega I - H(\mathbf{k}) - \Sigma(\mathbf{k},\omega)\big)^{-1}\Big|_{nn'}, \tag{41}$$

where $H(\mathbf{k})$ is a diagonal matrix containing the Kohn-Sham eigenvalues and $\Sigma(\mathbf{k},\omega)$ is non-diagonal (see above). The local Green function is simply

$$G^{\text{loc}}_{mm'}(\omega) = \sum_{\mathbf{k}} \langle \chi_{\mathbf{k}m} | \Psi_{\mathbf{k}n} \rangle \, G_{nn'}(\mathbf{k},\omega) \, \langle \Psi_{\mathbf{k}n'} | \chi_{\mathbf{k}m'} \rangle. \tag{42}$$

This equation is the generalization of Eq. (19).

The Self-Consistency Condition The DMFT self-consistency relation equals the local Green function and the Green function of the Anderson model:

$$G^{\text{loc}}_{mm'}(\omega) = G^{\text{Anderson}}_{mm'}(\omega) \tag{43}$$

where

$$G^{\text{Anderson}}_{mm'}(\omega) = \big(\omega I - E_0 - \Delta(\omega) - \Sigma(\omega)\big)^{-1}\Big|_{mm'}. \tag{44}$$

E_0 is a diagonal matrix with the levels of correlated orbitals in the (multiorbital) Anderson model, Σ and Δ are the self-energy and hybridization matrices in the correlated orbital basis. E_0 and Δ are obtained from the self-consistency condition.

The Anderson impurity model E_0, Δ and U, J define the Anderson model. The solution of the Anderson model gives the local self-energy, which is used again to compute the lattice Green function, Eq. (41).

The DFT loop The density can be obtained from the full Green function using:

$$n(\mathbf{r}) = -i \sum_{n,\mathbf{k}} \Psi_{\mathbf{k}n}(\mathbf{r}) \, G_{nn'}(\mathbf{k}, t - t' = 0^-) \, \Psi_{\mathbf{k}n'}(\mathbf{r}) \tag{45}$$

and is used to reconstruct the Kohn-Sham Hamiltonian (a functional of the density) and thus the eigenvalues. The scheme is summarized in Fig. 12.

2.2.4 Solvers for the Anderson impurity model

The resolution of the Anderson impurity model, Eq. (10), can be done by several methods. Simplifications can be done in some cases. In some localized systems (e.g. lanthanide oxides), one can neglect the bath in the resolution of the Anderson model. In this case, the hybridization and crystal field play a role only through the renormalization of the atomic levels. This is the basis of the Hubbard I method.

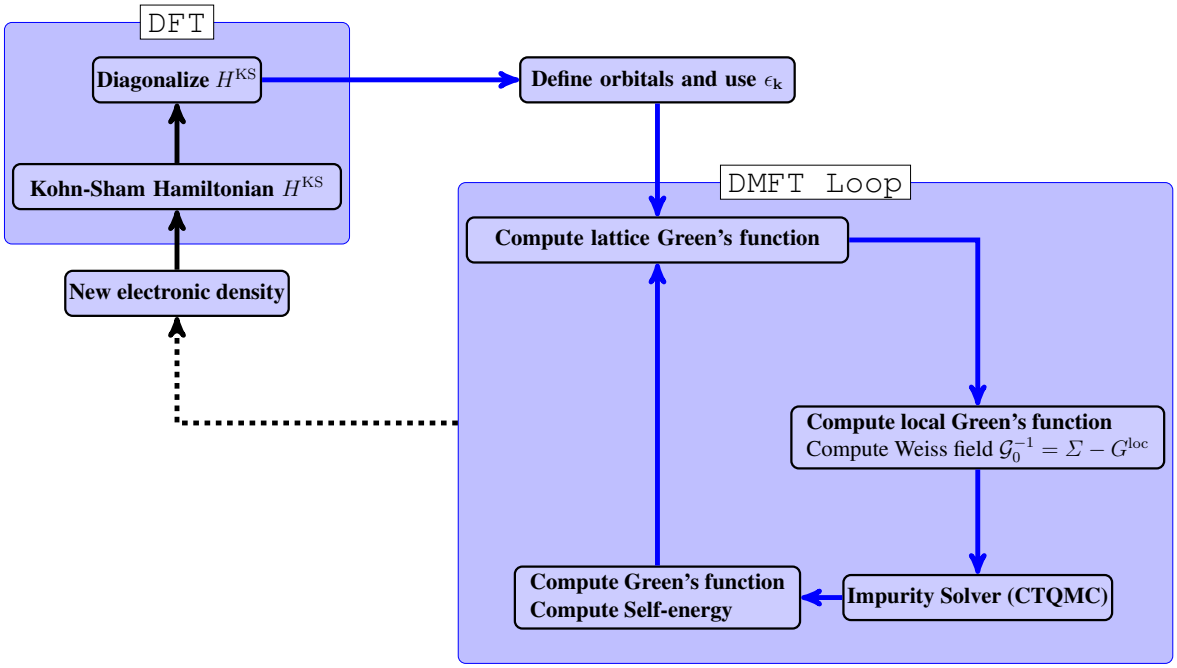

Fig. 12: *Scheme of the DFT+DMFT loops. $\mathcal{G}_0$ is the non-interacting Green function of the Anderson model and is linked to the hybridization by $\mathcal{G}_0^{-1} = \omega I - E_0 - \Delta(\omega)$. The Dyson Equation is $\mathcal{G}_0^{-1} - G^{-1} = \Sigma$.*

A more drastic solution is the static mean-field solution, which is equivalent to the DFT+U method [19]. To briefly present this approach, we suppose that density matrix of correlated orbitals is diagonal and $J = 0$. In this case, the self-energy for orbital i is simply $U(n_i - 1/2)$. It has the effect of opening a gap in Mott insulators by shifting occupied states downwards and empty states upward (see also [27]). However, even the atomic physics is not recovered and e.g paramagnetic insulators cannot be described with this approach. Some approximations can also be made if the system is on the metallic side (e.g. the Gutzwiller approximation).

In the general case, the solution can be provided by quantum Monte Carlo methods. The main idea is that the atomic problem can be solved exactly and the bath problem can be solved exactly. Most continuous-time quantum Monte Carlo codes, but not all, use an expansion as a function of H_1 in Eq. (10) and sample all relevant terms in the expansion.

2.2.5 Conclusion on DFT+DMFT

In this section, I have first reminded that the Hubbard model describes localization/delocalization transitions. Then I have presented the mapping to the Anderson model, and the DMFT equations. For real systems, I underlined that correlated orbitals and effective interactions have to be defined. Lastly, I detailed the DFT+DMFT scheme. The next section is devoted to applications to f-electron systems.

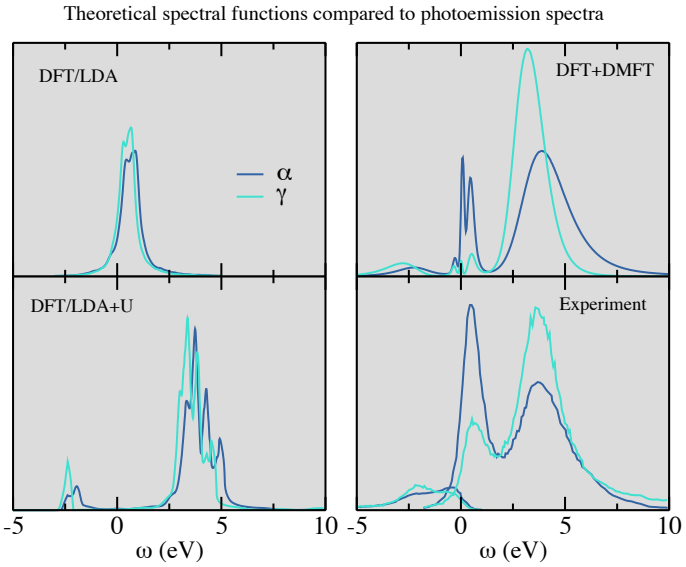

Fig. 13: *Theoretical spectral functions of cerium compared to photoemission spectra [9, 10]. Both the LDA and LDA+U spectra [28] are unable to differentiate the two phases of cerium. LDA+DMFT [29] describes qualitatively the appearance of the noticeable quasiparticle peak in the α-phase.*

3 f-electron systems: pure metals

3.1 Lanthanides

As discussed in the first section, f-electrons in lanthanides are localized and do not participate to the bonding at ambient pressure. So indeed, as DFT+DMFT correctly describes the atomic limit and the metal insulator transition, it should be adopted to describe these systems and their behavior under pressure. We will review in this section, photoemission, optical properties, magnetic and structural properties as described by DFT+DMFT on lanthanides.

3.1.1 Photoemission spectra

In this section, we discuss photoemission spectra of two lanthanides: cerium and terbium. For cerium, direct and inverse photoemission spectra were measured for both phases [9, 10] and are reproduced in Fig. 13. Importantly, both phases exhibit high-energy structures that can be interpreted as Hubbard bands. Only the α-phase has a sizable peak at the Fermi level, which suggests that the $4f$ electron is partly delocalized. We now compare to spectral functions obtained in DFT, DFT+U, and DFT+DMFT. We see that only DFT+DMFT is able to describe the important differences between the spectra of the α- and γ-phases, in contrast to LDA+U and LDA. LDA only describes the quasiparticle peak whereas LDA+U only opens a gap in the f-bands and thus describes only Hubbard bands.

We now discuss terbium spectra. Locht *et al.* [30] have computed photoemission spectra of all lanthanides using DFT+DMFT. At ambient pressure as discussed above, electrons are localized

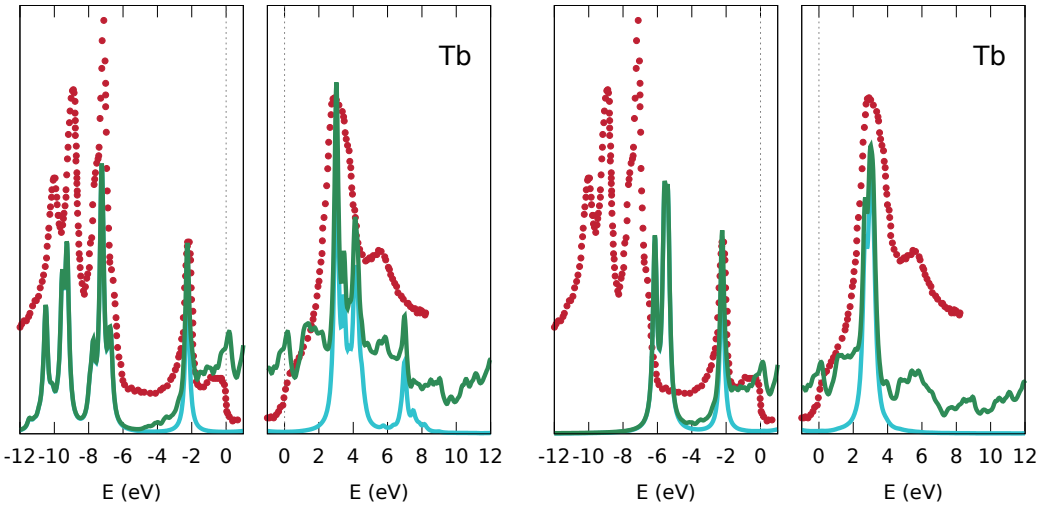

Fig. 14: *Comparison between experimental spectra (red dots) and the spectra calculated with DFT+DMFT (left) and with DFT+U (right). The green line is the calculated total spectral function. The blue line is the calculated $4f$ contribution to the spectral function [30].*

so the authors used the Hubbard I approximation. Fig. 14 shows theoretical spectra computed in DFT+DMFT and DFT+U compared to experimental spectra in the example of terbium. The direct photoemission spectrum contains peaks corresponding to the f^7 multiplets whereas inverse photoemission corresponds to f^9 states. These atomic features are correctly described by DMFT, provided that effective interactions and double-counting is correctly adjusted. In comparison, static mean-field LDA+U describes the system with only one Slater determinant and cannot reproduce the experimental data.

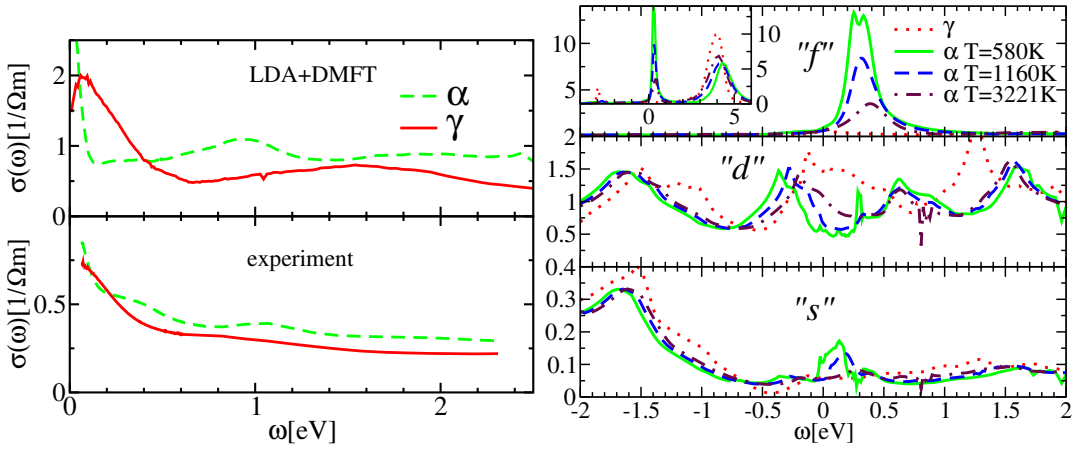

Fig. 15: *(left): calculated and experimental optical conductivity of phases of cerium (from [31]). (right): from top to bottom: f and d spectral functions, and hybridization function [31].*

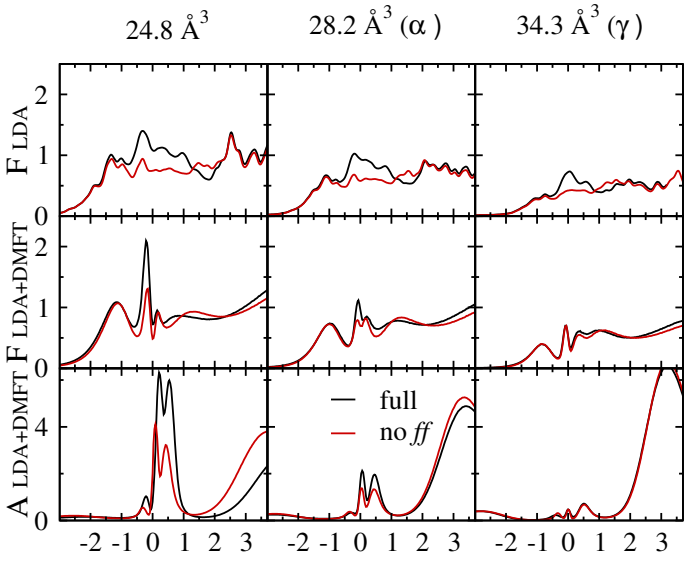

Fig. 16: *LDA and LDA+DMFT hybridizations and LDA+DMFT spectral function for three volumes of fcc cerium, including the α- and γ-phases [32].*

3.1.2 Optical conductivity

In Fig. 15, the experimental optical conductivity spectra of α- and γ-cerium are compared to DFT+DMFT calculations [31]. The DFT+DMFT calculations successfully reproduce the larger Drude peak in the γ-phase and the 1 eV peak in the α-phase spectra. The right panel of Fig. 15 provides insight into these spectra and the origin of these features. Indeed, at low temperature, when the quasiparticle f-peak at the Fermi level is large, the hybridization between f- and d-electrons creates a pseudo-gap in the d density of states, explaining the 1 eV peak in the α-phase. The large Drude peak at the Fermi level originates from the unhybridized d spectral function. This peak is visible mainly in the γ-phase where there is no pseudo-gap and thus an important d-weight at the Fermi level.
Two simplified models exist to describe the α-γ phase transition in cerium. They differ by the orbitals involved in the delocalization of f-electrons under pressure. The Mott transition assumes the f-f hoppings variation is most important, whereas in the Kondo Volume Collapse, it is the f-c hoppings that are dominant (c stands for s, p or d orbitals). The above analysis suggests that the main hybridization that drives the delocalization of f-electrons under pressure is the f-d hybridization. This is compatible with the qualitative view of strongly localized f-orbitals that have weak overlap.

3.1.3 Electronic model for the transition

To complement the above analysis, it is possible to simulate photoemission spectra with or without f-f hoppings to check the importance of this term. Fig. 16 shows the evolution of the $4f$ hybridization computed in LDA (top row), and LDA+DMFT (middle row), and the spectral functions computed in LDA+DMFT (bottom row) as a function of volume (in black). In

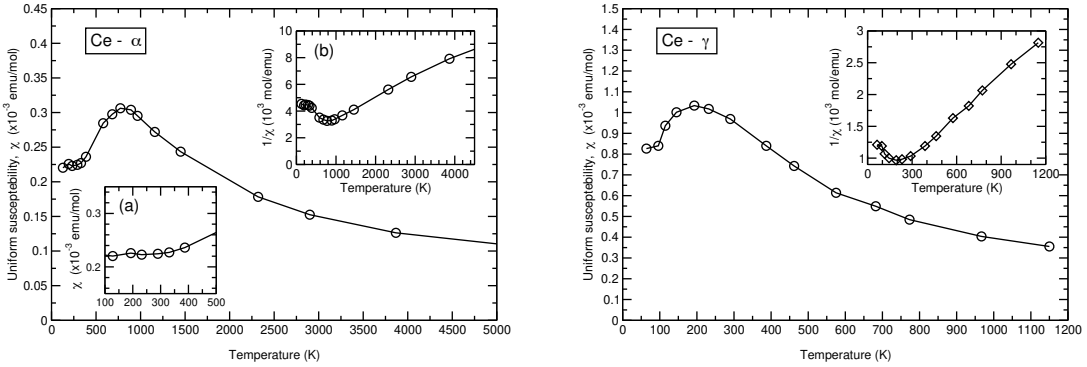

Fig. 17: *Magnetic susceptibility computed in DFT+DMFT [34] as a function of temperature for α- and γ-phases of cerium. We can analyze these data with the help of the phase diagram of Ce (Fig. 3). The magnetic susceptibility is constant as a function of temperature in the α-phase (below 500 K), whereas it has a Curie-Weiss behavior in the γ-phase (above 150 K). The γ-phase has thus a local moment. This is in qualitative agreement with experiment [33].*

red the same quantity is plotted without f-f hoppings [32]. The comparison of the hybridizations shows that f-c hybridization is clearly dominant at all volumes. Nevertheless, for lower volumes, the f-f hoppings play an increasing role in the amplitude of the hybridization. The amplitude of the quasiparticle peak is also impacted by the f-f hopping. This highlights that both hybridizations have to be taken into account and thus the need to go beyond models for a quantitative description of cerium.

3.1.4 Magnetism

Fig. 17 reproduces the magnetic susceptibility of cerium calculated within DFT+DMFT [34]. It exhibits a Curie-Weiss susceptibility at high temperature and low pressure in the γ-phase. This is in agreement with the spectral functions, that show mainly Hubbard bands and no quasiparticle peak, and suggest that this system is localized. In the α-phase, the quasiparticle peak is present, and a Pauli-like behavior in the α-phase (at low temperature) is observed. This is in qualitative agreement with experiments from Ref. [33].

3.1.5 Equation of states

Regarding cerium, numerous studies have extensively investigated the thermodynamics of its transition, highlighting the profound interplay between thermodynamic and electronic properties within the framework of density functional theory combined with dynamical mean-field theory (DFT+DMFT). Notably, these investigations have clearly demonstrated that the presence of a quasiparticle peak in the α-phases contributes to the stabilization of the phase at low temperatures. The inclusion of entropy and spin-orbit coupling has been found crucial for accurately describing the equation of states. In Fig. 18, the internal energy, entropy, and free energy at the transition are depicted, both with and without consideration of spin-orbit coupling. Let us start by discussing the internal energy. In both sets of calculations conducted within the volume range of the transition, we observe a softening of the energy's second derivative, indicating a

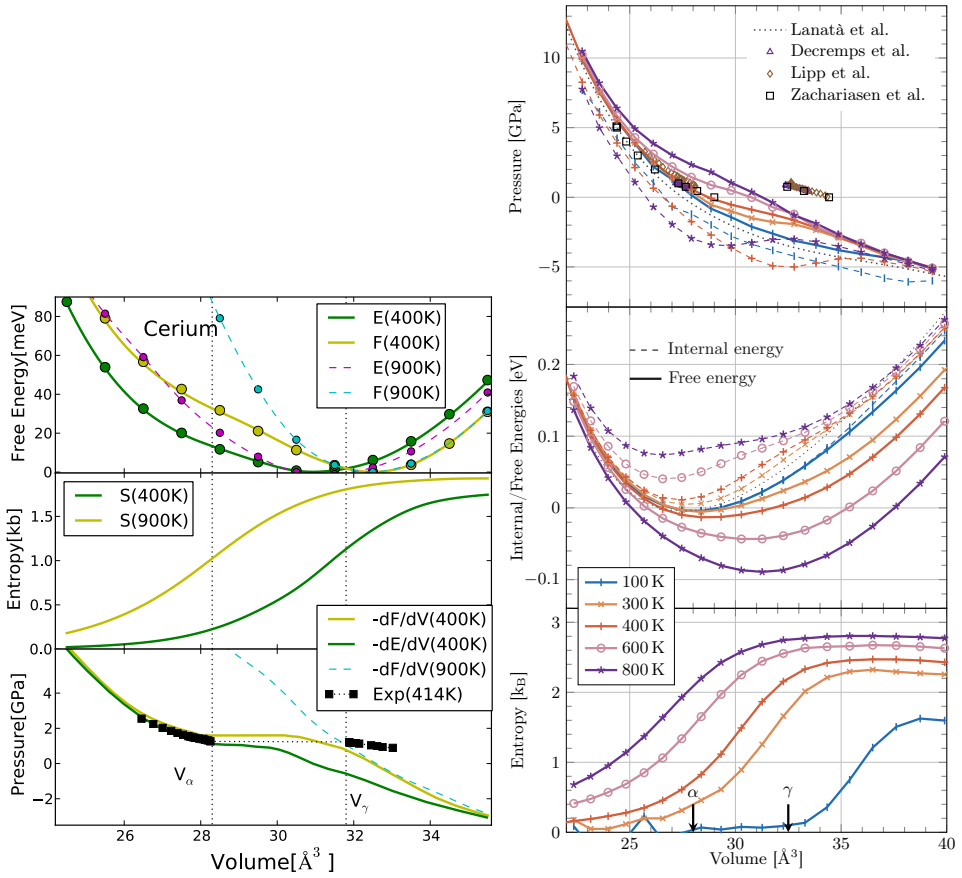

Fig. 18: *Internal, free energy, entropy, and pressure as a function of volume compared to experiment with spin-orbit coupling [35] and without spin-orbit coupling [29].*

decrease in the bulk modulus. However, it is crucial to consider the contribution of entropy, as its magnitude plays a significant role. It is worth noting that this magnitude is influenced by the degeneracy of the f-levels, which in turn depends on the inclusion of spin-orbit coupling. Finally, the resulting free energy exhibits a negative curvature, which is an indication of the presence of a phase transition. Notably, this distinctive feature is observed solely in the calculation that incorporates spin-orbit coupling. In this particular case, one can deduce the equation of state, which demonstrates a good agreement with the experimental equation of state.

3.2 Actinides

3.2.1 Structural properties

As discussed above, the volumes of actinides show a jump along the line. Uranium and neptunium have a low volume and a low symmetry structure whereas americium and curium have a large volume and compact phases. So plutonium is at the transition between two types of behavior. Depending on the temperature, it can exhibits low symmetry phase with low volume (α) or compact phase with high volume (δ). Concerning magnetism, all phases are non-magnetic, and there is no local moment except for curium.

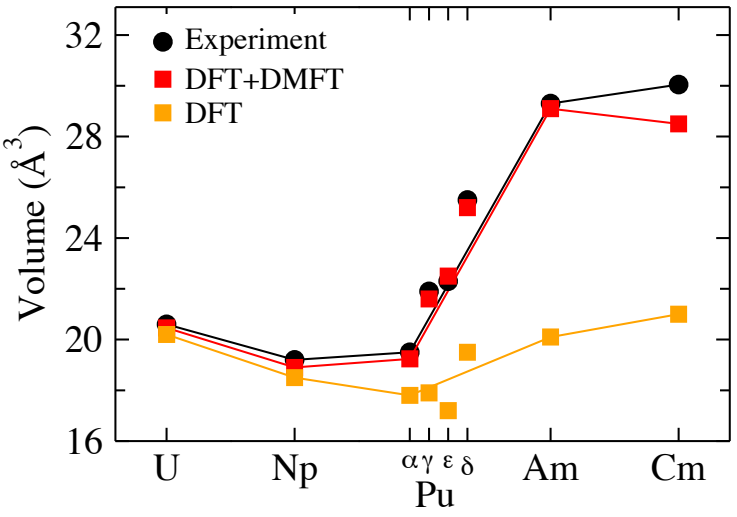

Fig. 19: *Volumes of uranium, neptunium, various phases of plutonium, americium and curium computed in non-magnetic GGA and DFT+DMFT [36].*

We now discuss theoretical results [36] reproduced on Fig. 19. GGA fails to recover the volume jump in actinides, unless an artificial magnetism is taken into account [36]. On contrary, DFT+DMFT is able to describe this transition. Interestingly spin-orbit coupling and Hund's exchange play a key role in this transition. In particular it is noticeable that the volume jump happens near the complete filling of the $J=5/2$ shell. This can be interpreted as an enhancement of correlation near the filling of this shell.

3.2.2 Branching ratio and importance of spin-orbit coupling

X-ray absorption spectroscopy (XAS) is especially useful to study f-electron systems because, as we will see below, it gives indication on the strength of the spin-orbit coupling (SOC). We focus here on the $4d$ to $5f$ transition. Spin-orbit coupling is very important for core states. So $4d$ orbitals are largely split in $4d_{5/2}$ and $4d_{3/2}$. $5f$ orbitals are less split by SOC. The absorption intensities $I_{5/2}$ and $I_{3/2}$, which correspond to $4d_{5/2} \rightarrow 5f_{5/2,7/2}$ and $4d_{3/2} \rightarrow 5f_{5/2}$ transitions, enable to define the branching ratio as $B = I_{5/2}/(I_{5/2} + I_{3/2})$. One can show that it is directly linked to the average of the spin-orbit operator. We can thus compare the experimental values of this operator to exact limits computed in the Russel-Saunders coupling scheme or the jj coupling scheme, and to ab-initio calculations. In the LS (Russel-Saunders) picture (see Fig. 20), we have in particular a cancellation of the spin-orbit coupling when $L=0$ for $n_f=7$. Whereas in jj coupling, the value increases until the $j=5/2$ shell is filled, after which it decreases.

Experimentally, the value is rather close to the jj case, except near $n_f=7$ where the stabilization of the half filled shell decreases the value of the spin-orbit operator. In Fig. 20, we compare the experimental value to LDA and LDA+DMFT calculations [37]. LDA overestimates the bandwidth, so the value of the spin-orbit coupling is underestimated. LDA+DMFT improves the agreement with experiment. This emphasizes the fact that LDA+DMFT correctly captures atomic physics.

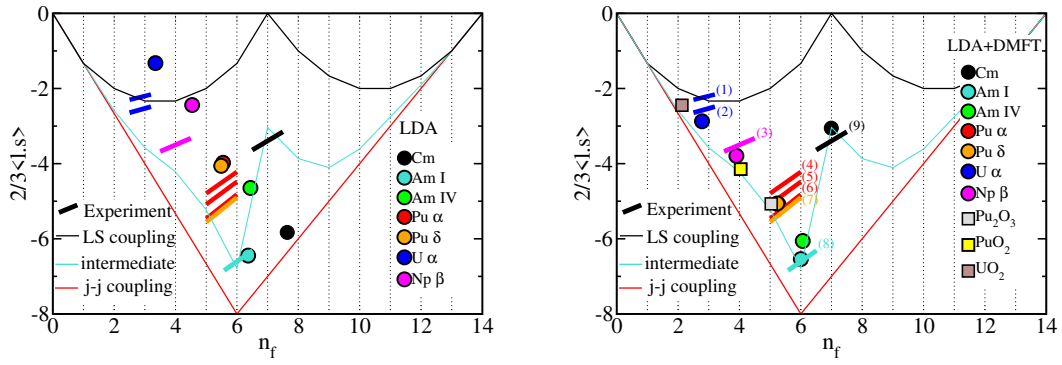

Fig. 20: *Value of spin-orbit operator deduced from the experimental branching ratio compared to exact limit (LS and jj coupling) and LDA (left) or LDA+DMFT (right) [37]*

4 f-electron systems: oxides

Most f-electron oxides are Mott insulators, and thus DFT+DMFT is the method of choice to describe them. DFT+U does describe also very well the structural and spectral properties, but not the magnetic properties. We will illustrate this with two examples of Mott insulators.

4.1 Electronic structure of Ce_2O_3

Ce_2O_3 is a Mott antiferromagnetic insulator with an optical band gap of 2.4 eV [61] and a Néel temperature of 9 K. We discuss in the following first the density of states and experiments, and secondly, the ground state density.

4.1.1 Density of states

Ce_2O_3 contains only one f-electron, resulting in the absence of multiplets in this system. Both DFT+U and DFT+DMFT methodologies successfully reproduce the energy gap of this compound. Fig. 21 shows the spectral function in DFT+DMFT. The DFT+U spectrum is very similar. These methods accurately capture the magnitude of the band gap which is between the two Hubbard bands. However, as we will discuss below, beneath these apparent similarities lie profound differences between the two approaches.

4.1.2 Electronic Density

To illustrate the differences between the LDA+DMFT and LDA+U electronic densities, we have plotted in Fig. 22 the isosurfaces of the differences between the LDA+DMFT and LDA electronic densities (on the left) and between LDA+U and LDA electronic densities (on the right). We see that the difference between LDA+DMFT and LDA is weaker than the difference between LDA+U and LDA. This suggests that the occupation matrices of the correlated orbitals are different in LDA+U and LDA+DMFT.

We now explain the origin of this difference. In DFT, local interaction is not taken into account, so the f-electron is delocalized over several f-orbitals. In DFT+U, because of the localization,

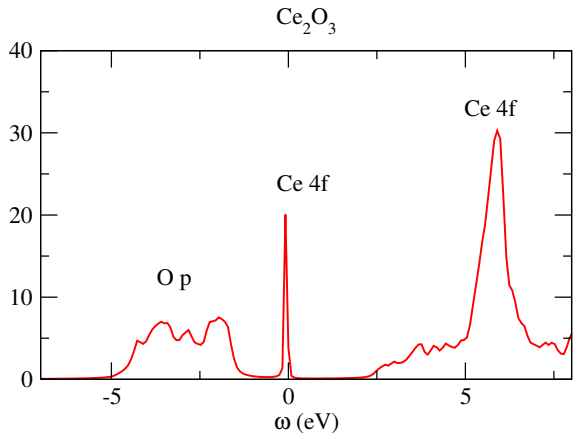

Fig. 21: *DFT+DMFT spectral function of Ce_2O_3 [38]*

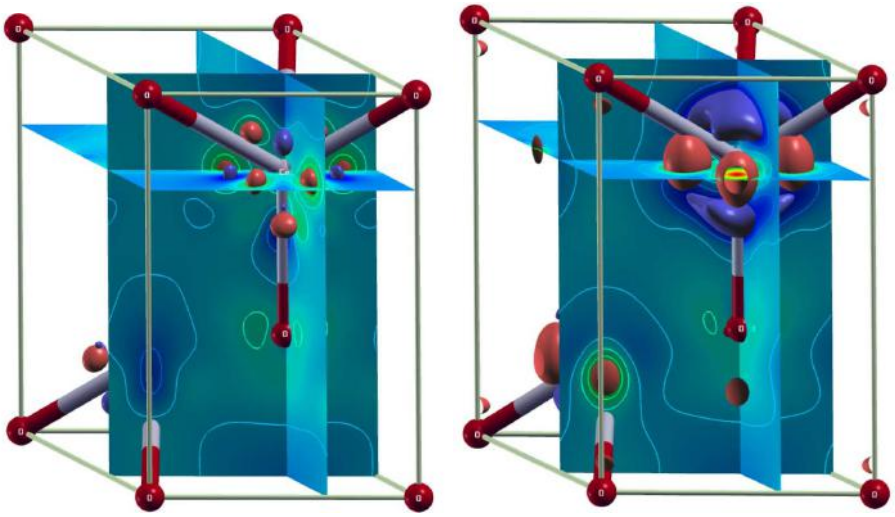

Fig. 22: *Difference between the electron densities computed using LDA+U (right) and LDA+DMFT (left) approximations and in the LDA approximation. The density of the filled orbital is clearly visible on the right. The blue (respectively green-red) area corresponds to a positive (respectively negative) value of the difference. [38]*

numerous low-energy one-electron nearly-degenerate states are present in these systems. Each of these states can be calculated using a single Slater determinant method like DFT+U [39] and corresponds to the localization of the f-electron in one f-orbital. As a consequence, the average occupation of one orbital is either close to 0 or 1 (to reduce the Coulomb interaction). This explains the large difference of the electron densities between DFT+U and DFT as seen in the right plot of Fig. 22.

However, to accurately describe a paramagnetic insulator without introducing unwanted orbital anisotropy and magnetism, a method capable of handling multiple determinants, such as DFT+DMFT, is required. In DFT+DMFT, the instantaneous occupation of orbitals is 0 or 1. But the average occupations of f-orbitals are lower and closer to the DFT/LDA values. The left plot of Fig. 22 highlights the similarity of the DFT/LDA and DFT+DMFT densities, even if it comes from completely different physical effects.

4.2 Magnetic ordering in UO_2

As f-orbitals are particularly localized, they are less sensitive to crystal-field effects. As a consequence, the orbital angular momentum is not quenched and plays an important role in magnetism. In particular, multipolar degrees of freedom can play a role: their interactions can lead to ordering of their arrangement.
This has been studied in UO_2 to resolve the long standing question of the 3**k** magnetic order in the antiferromagnetic phase, below 30 K. This peculiar ordering involves 4 different orientations of magnetic moments. Pourovkii *et al.* [40] proposed to compute nearest-neighbor interactions between the states belonging to the Γ_5 ground state using DFT+DMFT. DFT+DMFT describes well the band structure and paramagnetism in UO_2 [26]. Using the Hubbard I approximation, they were able to compute superexchange parameters for dipolar and quadrupolar interactions. Using these interactions, they were able to stabilize the experimental magnetic ordering and the phase transition to paramagnetism at a temperature close to experiment. Another recent work used a flavor of DFT+U to show the role of quadrupolar-quadrupolar interactions in the formation of 3**k** magnetic order.

5 Conclusion

f-electron systems exhibit significant orbital localization for lanthanides and comparatively lesser localization for actinides. As a consequence electrons are sensitive to electronic interaction and somewhat less to crystal fields in comparison to the d-elements. Spin-orbit coupling is also important for these heavy elements. These features require a good description of atomic physics and hybridization, which is provided by DFT+DMFT.

References

[1] A. Georges, G. Kotliar, W. Krauth, and M.J. Rozenberg, Rev. Mod. Phys. **68**, 13 (1996)

[2] G. Kotliar, S.Y. Savrasov, K. Haule, V.S. Oudovenko, O. Parcollet, and C.A. Marianetti, Rev. Mod. Phys. **78**, 865 (2006)

[3] A. Georges, AIP Conf. Proc. **715**, 3 (2004)

[4] S. Hecker, Metall. Mater. Trans. A **35**, 2207 (2004)

[5] A. McMahan, C. Huscroft, R. Scalettar, and E. Pollock, J. Comput. Aided Mater. Des. **5**, 131 (1998)

[6] A. Schiwek, F. Porsch, and W.B. Holzapfel, U. Krell, J.R. Schneider, M. von Zimmermann (eds.): Scientific Contributions. Part 1, HASYLAB Annual Report Hamburg, 2002

[7] F. Decremps, L. Belhadi, D.L. Farber, K.T. Moore, F. Occelli, M. Gauthier, A. Polian, D. Antonangeli, C.M. Aracne-Ruddle, and B. Amadon, Phys. Rev. Lett. **106**, 065701 (2011)

[8] B. Johansson, W. Luo, S. Li, and R. Ahuja, Sci. Rep. **4**, (2014)

[9] E. Weschke, C. Laubschat, T. Simmons, M. Domke, O. Strebel, and G. Kaindl, Phys. Rev. B **44**, 8304 (1991)

[10] M. Grioni, P. Weibel, D. Malterre, Y. Baer, and L. Du'o, Phys. Rev. B **55**, 2056 (1997)

[11] P.W. Anderson, Phys. Rev. **124**, 41 (1961)

[12] P. Fulde, J. Phys. F: Metal Phys. **18**, 601 (1988)

[13] E. Pavarini and E. Koch (Eds.): *Simulating Correlations with Computers*, Modeling and Simulation, Vol. 10 (Forschungszentrum Jülich, 2011) `http://www.cond-mat.de/events/correl21`

[14] V.I. Anisimov, D.E. Kondakov, A.V. Kozhevnikov, I.A. Nekrasov, Z.V. Pchelkina, J.W. Allen, S.-K. Mo, H.-D. Kim, P.Metcalf, S. Suga, A. Sekiyama, G. Keller, I. Leonov, X. Ren, and D. Vollhardt, Phys. Rev. B **71**, 125119 (2005)

[15] F. Lechermann, A. Georges, A. Poteryaev, S. Biermann, M. Posternak, A. Yamasaki, and O.K. Andersen, Phys. Rev. B **74**, 125120 (2006)

[16] B. Amadon, F. Lechermann, A. Georges, F. Jollet, T.O. Wehling, and A.I. Lichtenstein, Phys. Rev. B **77**, 205112 (2008)

[17] F. Aryasetiawan, M. Imada, A. Georges, G. Kotliar, S. Biermann, and A.I. Lichtenstein, Phys. Rev. B **70**, 195104 (2004)

[18] N. Marzari and D. Vanderbilt, Phys. Rev. B **56**, 12847 (1997)

[19] V.I. Anisimov and O. Gunnarsson, Phys. Rev. B **43**, 7570 (1991)

[20] M. Cococcioni and S. de Gironcoli, Phys. Rev. B **71**, 035105 (2005)

[21] L. Vaugier, H. Jiang, and S. Biermann, Phys. Rev. B **86**, 165105 (2012)

[22] E. Pavarini, E. Koch, D. Vollhardt, A. Lichtenstein (Eds.):
The LDA+DMFT approach to strongly-correlated materials,
Modeling and Simulation, Vol. 1 (Forschungszentrum Jülich, 2011)
`http://www.cond-mat.de/events/correl11`

[23] B. Amadon, T. Applencourt, and F. Bruneval, Phys. Rev. B **89**, 125110 (2014)

[24] P. Seth, P. Hansmann, A. van Roekeghem, L. Vaugier, and S. Biermann,
Phys. Rev. Lett. **119**, 056401 (2017)

[25] R. Sakuma and F. Aryasetiawan, Phys. Rev. B **87**, 165118 (2013)

[26] J. c. v. Kolorenč, A.B. Shick, and A.I. Lichtenstein, Phys. Rev. B **92**, 085125 (2015)

[27] E. Pavarini, E. Koch, F. Anders, and M. Jarrell (Eds.): *From Models to Materials*
Modeling and Simulation, Vol. 2 (Forschungszentrum Jülich, 2012)
`http://www.cond-mat.de/events/correl12`

[28] B. Amadon, F. Jollet, and M. Torrent, Phys. Rev. B **77**, 155104 (2008)

[29] J. Bieder and B. Amadon, Phys. Rev. B **89**, 195132 (2014)

[30] I.L.M. Locht, Y.O. Kvashnin, D.C.M. Rodrigues, M. Pereiro, A. Bergman, L. Bergqvist, A.I. Lichtenstein, M.I. Katsnelson, A. Delin, A.B. Klautau, B. Johansson, I. Di Marco, and O. Eriksson, Phys. Rev. B **94**, 085137 (2016)

[31] K. Haule, V. Oudovenko, S.Y. Savrasov, and G. Kotliar,
Phys. Rev. Lett. **94**, 036401 (2005)

[32] B. Amadon and A. Gerossier, Phys. Rev. B **91**, 161103 (2015)

[33] T. Naka, T. Matsumoto, and N. Môri, Physica B: Condensed Matter **205**, 121 (1995)

[34] S.V. Streltsov, E. Gull, A.O. Shorikov, M. Troyer, V.I. Anisimov, and P. Werner,
Phys. Rev. B **85**, 195109 (2012)

[35] K. Haule and T. Birol, Phys. Rev. Lett. **115**, 256402 (2015)

[36] B. Amadon, Phys. Rev. B **97**, 039903 (2018)

[37] J H. Shim, K. Haule, and G. Kotliar, EPL (Europhys. Lett.) **85**, 17007 (2009)

[38] B. Amadon, Journal of Physics: Condensed Matter **24**, 075604 (2012)

[39] B. Dorado, B. Amadon, M. Freyss, and M. Bertolus, Phys. Rev. B **79**, 235125 (2009)

[40] L.V. Pourovskii and S. Khmelevskyi, Phys. Rev. B **99**, 094439 (2019)